Membrane-Bound Orientation and Position of the Synaptotagmin C2B Domain Determined by Site-Directed Spin Labeling†

Elisabeth Rufener,‡ April A. Frazier,‡,§ Catherine M. Wieser,‖ Anne Hinderliter,‖ and David S. Cafiso*,‡

Department of Chemistry and Biophysics Program, University of Virginia, Charlottesville, Virginia 22904, and Department of Pharmaceutical Sciences, North Dakota State University, Fargo, North Dakota 58105

Received July 30, 2004; Revised Manuscript Received October 15, 2004

ABSTRACT: Site-directed spin labeling is used to determine the orientation and depth of insertion of the second C2 domain from synaptotagmin I (C2B) into membrane vesicles composed of phosphatidylcholine (PC) and phosphatidylserine (PS). EPR line shapes of spin-labeled mutants located with the Ca^{2+}-binding loops of C2B broaden in the presence of Ca^{2+} and PC/PS vesicles, indicating that these loops undergo a Ca^{2+}-dependent insertion into the membrane interface. Power saturation of the EPR spectra provides a position for each spin-labeled site along the bilayer normal, and these EPR-derived distance constraints, along with a high-resolution structure of the C2B domain, are used to generate a model for the domain orientation and position at the membrane interface. Our data show that the isolated C2B domain from synaptotagmin I penetrates PC/PS membranes, and that the backbone of Ca^{2+}-binding loops 1 and 3 is inserted below the level of a plane defined by the lipid phosphates. The side chains of several loop residues are within the bilayer interior, and both Ca^{2+}-binding sites are positioned near a plane defined by the lipid phosphates. A Tb^{3+}-based fluorescence assay is used to compare the membrane affinity of the C2B domain to that of the first synaptotagmin C2 domain (C2A). Both C2A and C2B bind PC/PS (75:25) membrane vesicles with a micromolar lipid affinity in the presence of metal ion. These results indicate that C2A and C2B have a similar membrane affinity and position when bound to PC/PS (75:25) membrane vesicles. EPR spectroscopy indicates that the C2B domain has different interactions with PC/PS membranes containing 1 mol % phosphatidylinositol 4,5-bisphosphate.

In the central nervous system, neurotransmission and intercellular information flow are dependent upon regulated membrane fusion. Fusion in these cells is a tightly coordinated, Ca^{2+}-triggered process that is facilitated by a large number of protein components. The SNARE[1] protein complex is a four-helix bundle that tethers the synaptic vesicle to the presynaptic membrane, and the assembly of this complex is essential to the fusion event. However, the SNAREs do not directly bind Ca^{2+}, and there is substantial evidence that the Ca^{2+}-dependent trigger in this process is synaptotagmin I, a synaptic vesicle-associated membrane protein that contains two C2 domains (for reviews, see refs *1* and *2*). Synaptotagmin I is a 421-amino acid, 47 kDa protein that is anchored to the synaptic vesicle membrane by a single transmembrane helical segment near its N-terminus. The two C2 domains of synaptotagmin I (termed C2A and C2B) are C-terminal to this membrane helical segment in the cytoplasm. There is compelling evidence that these C2 domains form the Ca^{2+}-sensing elements for neuronal exocytosis (*3*−*7*), and recent evidence has been obtained indicating that synaptotagmin I and the SNAREs constitute a minimal protein machinery necessary for Ca^{2+}-regulated membrane fusion (*8*).

C2 domains are found in a wide range of proteins that function in cell signaling and are recognized as one of the most prevalent Ca^{2+}-binding motifs in eukaryotic systems (*9*−*11*). The C2 domain generally functions to attach proteins to membranes in a Ca^{2+}-dependent fashion, although several isoforms associate with membranes in a Ca^{2+}-independent manner (*12*). Figure 1 shows the average NMR-derived solution structure of the isolated synaptotagmin C2B domain (*13*). As shown in Figure 1, the Ca^{2+}-binding sites in C2 domains are located in the loops that connect the β-strands on one end of an eight-stranded β-sandwich, and in cases where the membrane interactions of C2 domains have been determined, the Ca^{2+}-binding loops are the sites that interact with the membrane interface (*14*−*18*).

† This work was supported by NIH Grants GM62305 (D.S.C.) and GM64443 (A.H.) and the ACS Petroleum Research Fund type G (A.H.).

* To whom correspondence should be addressed: Department of Chemistry, University of Virginia, Charlottesville, VA 22904-4319. E-mail: cafiso@virginia.edu. Telephone: (434) 924-3067. Fax: (434) 924-3567.

‡ University of Virginia.

§ Present address: Department of Pharmacology, University of Iowa, Iowa City, IA 52242.

‖ North Dakota State University.

[1] Abbreviations: bR, bacteriorhodopsin; AEBSF, aminoethylbenzene sulfonyl fluoride hydrochloride; CBL, Ca^{2+}-binding loop; DPPH, α,α′-diphenyl-β-picrylhydrazyl; ENTH, epsin N-terminal homology; EPR, electron paramagnetic resonance spectroscopy; HEPES, *N*-(2-hydroxyethyl)piperazine-*N*′-2-ethanesulfonic acid; LUV, large unilamellar vesicle; MOPS, morpholinopropanesulfonic acid; MTSL, methanethiosulfonate spin-label; NiEDDA, nickel(II) ethylenediaminediacetic acid; $PI(4,5)P_2$, phosphatidylinositol 4,5-bisphosphate; PH, pleckstrin homology; PMSF, phenylmethanesulfonyl fluoride; PKC, protein kinase C; PLC-δ, phospholipase C; cPLA2, cytosolic phospholipase A_2-α; PC, phosphatidylcholine; POPC, palmitoyloleoylphosphatidylcholine; POPS, palmitoyloleoylphosphatidylserine; PS, phosphatidylserine; SDSL, site-directed spin labeling; sytIC2A, synaptotagmin I C2A domain; sytIC2B, synaptotagmin I C2B domain; SNAREs, soluble *N*-ethylmaleimide-sensitive factor attachment proteins.

10.1021/bi048370d CCC: $30.25
Published on Web 12/08/2004

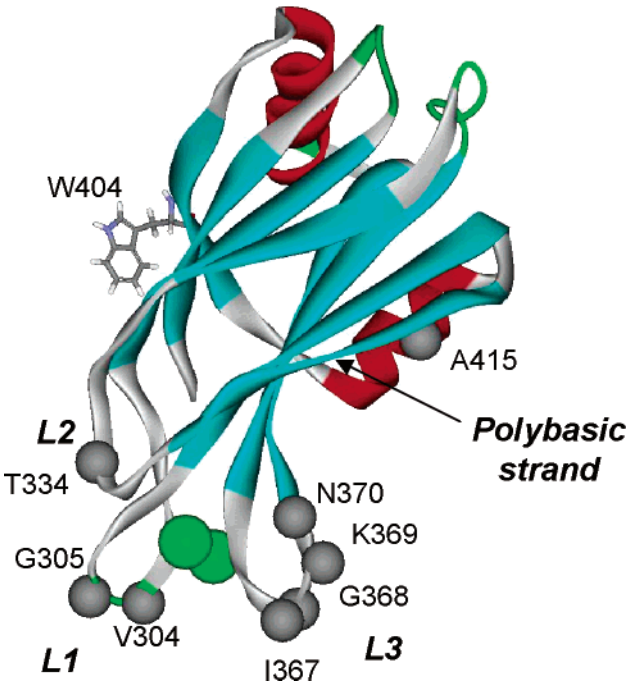

FIGURE 1: Average structure of the synaptotagmin I C2B domain obtained by high-resolution NMR (PDB entry 1KW5) (*13*). The three loops on one end of the domain that form the Ca^{2+}-binding sites are labeled (L1−L3) along with two bound Ca^{2+} ions. Also shown is β-strand 4, which contains a number of positively charged side chains and is termed the polybasic strand. The C-terminal helix of C2B lies near this polybasic strand. The Cα positions that are derivatized with spin-labels in this study are shown along the backbone of the domain. The tryptophan at position 404 was used to probe binding of Tb^{3+} to the Ca^{2+} sites through energy transfer.

The Ca^{2+}-dependent membrane binding properties of both the synaptotagmin I C2A and C2B domains have been studied. The C2A domain binds membrane surfaces composed of phosphatidylcholine (PC) and phosphatidylserine (PS) in a Ca^{2+}-dependent manner with a micromolar lipid dissociation constant (*10*, *16*). When membrane-bound, this domain penetrates the membrane interface, and EPR spectroscopy places the polypeptide backbone of both the first and third Ca^{2+}-binding loops in contact with the membrane interface so that several side chains from loop residues project into the bilayer interior (*16*). The membrane binding properties of C2B have been more difficult to establish. Earlier work on C2B indicated that it did not function in Ca^{2+}-dependent membrane binding, but instead was involved in mediating protein−protein interactions (*11*, *19*). However, this lack of membrane binding was due to a nucleic acid contaminant that accompanied bacterial expression and purification (*20*). Once this contaminant was removed by an additional purification step, the isolated C2B domain was found to bind PC/PS membranes in a Ca^{2+}-dependent fashion.

Many proteins that are involved in membrane trafficking, such as the copines or tricalbins, appear to have multiple C2 domains (*21*, *22*). However, the function and role of these multiple domains are not understood. For synaptotagmin, recent work suggests that C2A and C2B may be specialized to bind to different membrane compositions (*23*). For example, the C2A domain expressed alone binds to PC/PS membranes with a micromolar lipid affinity, while the C2B domain expressed alone has been reported to have a much weaker affinity for PC/PS membranes (*23*). The C2A domain has been shown to penetrate lipid bilayers formed from PC and PS, but fluorescent labels placed within the first and third Ca^{2+}-binding loops indicate that the isolated C2B domain does not penetrate membranes containing PC and PS. On the other hand, the isolated C2B has been reported to bind and penetrate membranes containing PC and phosphatidylinositol 4,5-bisphosphate [$PI(4,5)P_2$], whereas isolated C2A does not (*24*).

In this report, both the membrane affinity and orientation of the isolated synaptotagmin I C2B domain (residues 249−421 of rat sytI) on PC/PS bilayers are examined. A Tb^{3+}-based fluorescence assay is used to show that C2B binds to membranes composed of PC and PS with an affinity comparable to that of C2A. SDSL and EPR spectroscopy are also used to determine the orientation and position of the C2B domain on the membrane interface. C2B is found to penetrate the bilayer interface and to assume an orientation and depth with respect to the interface similar to those of C2A. Within experimental error, the Ca^{2+} binding sites in C2B lie at approximately the same depth in the membrane interface as those of C2A. Thus, C2A and C2B interact in a similar manner with PC/PS membrane surfaces.

EXPERIMENTAL PROCEDURES

Materials. 1-Palmitoyl-2-oleoyl-*sn*-glycero-3-phosphocholine (POPC), 1-palmitoyl-2-oleoyl-*sn*-glycero-3-phosphoserine (POPS), and phosphatidylinositol 4,5-bisphosphate [$PI(4,5)P_2$] were obtained from Avanti Polar Lipids, Inc. (Birmingham, AL). The sulfhydryl reactive spin-label, (1-oxyl-2,2,5,5-tetramethyl-Δ^3-pyrroline-3-methyl) methanethiosulfonate (MTSL), was purchased from Toronto Research Chemicals, Inc. (North Fork, ON). The paramagnetic reagent, nickel(II) ethylenediamine-*N*,*N*′-diacetic acid (NiEDDA), was synthesized as described previously (*25*). GSTrap FF prepacked columns, benzamidine prepacked columns, the HiPrep desalting column, HiTrap Q HP columns, and thrombin protease were purchased from Amersham Biosciences (Piscataway, NJ). High-fidelity Vent DNA polymerase and all restriction endonucleases were obtained from New England Biolabs (Beverly, MA). Benzonase nuclease was purchased from Novagen (San Diego, CA).

Buffers. The buffers used included the following: PBS (phosphate-buffered saline), consisting of 10 mM Na_2HPO_4, 2.7 mM KCl, 1.8 mM KH_2PO_4, and 140 mM NaCl (pH 7.3); resuspension buffer, consisting of PBS, 5 mM EDTA, 0.5 mM AEBSF, 100 μM leupeptin, 50 units/mL aprotinin, 1% benzonase, and 2% Triton X-100; wash buffer, consisting of PBS, 1% Triton X-100, and 2 mM EDTA; prep buffer, consisting of 150 mM NaCl and 50 mM Tris Base (pH 8.4); cleavage buffer, consisting of 150 mM NaCl, 4.0 mM $CaCl_2$, and 50 mM Tris Base (pH 8.4); elution buffer, consisting of 750 mM NaCl, 25 mM EDTA, and 50 mM Tris Base (pH 8.4); QA buffer, consisting of 150 or 50 mM KCl, 50 mM MOPS, and 5 mM EDTA (pH 7.2); QB buffer, consisting of 800 mM KCl, 50 mM MOPS, and 5 mM EDTA (pH 7.2); and EPR buffer, consisting of 1 mM $CaCl_2$, 100 mM NaCl, and 50 mM HEPES (pH 7.2). Buffers used for fluorescence binding measurements were decalcified by passage of the 2× buffer [4 mM MOPS and 200 mM KCl (pH 7.5)] over a Chelex column before dilution. Terbium chloride hexahydrate (Molecular Probes, Inc., Eugene, OR), a stable hydrate,

Scheme 1

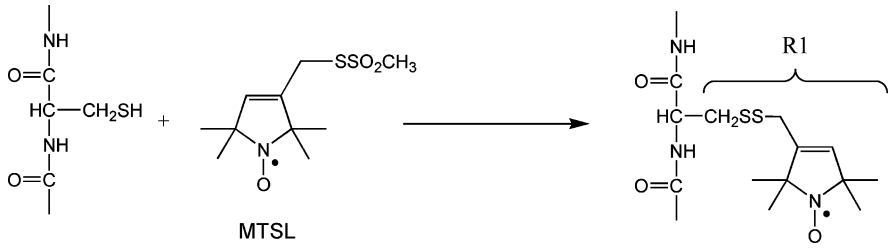

was prepared gravimetrically and hydrated in decalcified buffer.

Site-Directed Mutagenesis. The DNA of rat sytIC2B (P21707), in vector pGEX-KG (*26*) encoding amino acid residues 249−421, was provided by C. Creutz (Department of Pharmacology, University of Virginia). All DNA modifications followed published protocols (*27*). The single cysteine residue at position 277 was removed by typical polymerase chain reaction (PCR) strategies, and a two-step PCR method was used to generate eight single-cysteine mutants of C2B. Individual cysteine residues were introduced at positions 304 and 305 (in Ca^{2+}-binding loop 1), 334 (loop 2), 367, 368, 369, and 370 (in loop 3), and 415 in the C-terminal α-helix (see Figure 1). All cysteine substitutions were confirmed by DNA sequencing.

Protein Expression and Purification. The synaptotagmin I C2B domain was expressed and purified using a glutathione *S*-transferase fusion protein. To express the fusion protein, the mutant plasmids for sytIC2B were transformed into BL21(DE3)pLys*S* cells, and single colonies were used to inoculate 100 mL precultures of Luria-Bertani (LB) medium containing 50 mg/L ampicillin, which were grown for approximately 8 h at 37 °C. The preculture was used to inoculate a 900 mL culture of LB medium in a 2.8 L Fernbach flask, with 50 mg/L ampicillin, which was grown at 37 °C until an OD_{600} of 0.6−0.8 was reached. Expression was induced with 0.1 mM isopropyl β-D-thiogalactopyranoside, and growth was allowed to proceed for 4−6 h at 20 °C with vigorous shaking. The cells were collected by centrifugation at 9500*g* for 20 min at 4 °C, and the pellet was solubilized in resuspension buffer, lysed using a French press, and centrifuged at 15000*g* for 10 min at 4 °C. The clarified supernatant was preserved at 4 °C, for up to 1 week.

The fusion protein containing the sytIC2B domain was affinity purified from the clarified supernatant by chromatography on GSTrap FF prepacked columns using an AKTA Prime system (Amersham Biosciences, Piscataway, NJ). The clarified sytIC2B was filtered with a 0.22 μm syringe filter, added to the column, washed several times with wash buffer, and equilibrated with prep buffer. To remove the C2B domain from the column, the bound GST fusion protein was cleaved by adding thrombin in cleavage buffer. The column was allowed to incubate overnight at 4 °C, and the C2B domain was eluted from the column using elution buffer. The protein purity and identity were confirmed by SDS−PAGE (Bio-Rad, Hercules, CA). The molecular mass for sytIC2B was approximately 20 kDa, consisting of synaptotagmin residues 249−421 and 13 additional residues from the pGEX vector on the N-terminus.

At this stage, the affinity-purified C2B domain contains a bound nucleic acid contaminant, which is indicated by an optical absorbance maximum for the protein that is significantly less than 278 nm (typically between 260 and 270 nm). The C2B domain contains a highly charged polybasic region (see Figure 1) that appears to be responsible for binding polynucleotides (*20*). To remove this contaminant, the affinity-purified protein was first incubated with benzonase overnight at 4 °C to cleave the nucleic acid contaminant. Anion exchange chromatography was then performed to separate the contaminant from C2B. Following benzonase treatment, the protein was concentrated, buffer exchanged into QA buffer, loaded onto four HiTrap Q HP prepacked 5 mL columns in a series, and eluted with a gradient from 50 to 800 mM KCl (using QB buffer) over 4 column volumes. Following anion exchange, C2B had an absorbance maximum of 278 nm, indicating that the protein was largely free of nucleic acid contaminant (*20*). The protein was buffer exchanged into 0.5 mM ammonium bicarbonate, vacuum desiccated, and stored at −20 °C.

Spin Labeling sytIC2B. To spin-label the single-cysteine mutants, the protein was suspended in 1.5 mL of EPR buffer, and DTT was added at a DTT:protein mole ratio of 3:1. The methanethiosulfonate spin-label (MTSL) (see Scheme 1) was then added at a MTSL:DTT mole ratio of 10:1, and the mixture was gently mixed and stored without stirring in the dark at room temperature for 2 h. Excess spin-label was removed by passing the sample through a HiPrep 16/10 desalting column, and the protein was concentrated using a Centricon YM-10 ultrafiltration membrane (Millipore, Billerica, MA).

Large Unilamellar Vesicles. Large unilamellar vesicles (LUVs) were prepared with a POPC:POPS ratio of 75:25 as described previously (*16*). Briefly, the appropriate aliquots of lipids in either chloroform or chloroform and methanol were mixed; the solvent was removed by rotary evaporation, and the sample was vacuum desiccated overnight. The resulting film was hydrated in buffer without Ca^{2+} for 1 h, vortexed thoroughly, and extruded through a 0.1 μm pore diameter polycarbonate filter using a hand-held Mini-Extruder (Avanti Polar Lipids).

Fluorescence Estimates of C2B Domain Metal Ion and Membrane Affinity. The affinity of metal ion for the C2B domain was estimated by assessing the binding of Tb^{3+}, a Ca^{2+} analogue with an ionic radius similar to that of Ca^{2+} but a charge density higher than that of Ca^{2+}. Previously, this method produced metal ion and membrane binding affinities for sytIC2A that were consistent with previously published results (*16*). In addition, the EPR spectra of spin-labeled C2A mutants in the presence of membranes were identical whether terbium or calcium ions were used to induce binding.

When bound to the protein, Tb^{3+} may act as an acceptor of fluorescence energy from aromatic amino acids (*28*−*30*). To assess binding of Tb^{3+} to the C2B domain, the protein is

excited at 295 nm and the fluorescence of the single tryptophan at position 404 is monitored at 337 nm. The binding of Tb^{3+} results in a decrease in the typtophan fluorescence. This decrease in emission intensity, ΔF, as a function of the Tb^{3+} concentration was normalized to yield the fraction of metal ion sites bound, f_b, and the data were fit to the following expression:

$$f_b = \frac{\Delta F}{\Delta F_{max}} = \frac{([Tb^{3+}]/K_d)^n}{1 + ([Tb^{3+}]/K_d)^n} \quad (1)$$

where ΔF_{max} represents the maximal fluorescence change, n is the Hill coefficient, and K_d is the apparent dissociation constant for binding of Tb^{3+} to sytIC2B. The presence of lipid increased the affinity of protein for the terbium ion. This can be detected as a loss of protein fluorescence at lower cation concentrations and consequently a lower apparent dissociation constant, K_d. The Hill coefficient for cation binding was unchanged in the presence or absence of lipid (*31*).

The membrane affinities of C2A and C2B were compared by measuring the tryptophan fluorescence of each domain as a function of lipid concentration in the presence of subsaturating concentrations of Tb^{3+}. The decrease in tryptophan fluorescence with increasing concentrations of POPC/POPS (75:25) LUVs is a result of Tb^{3+} and membrane binding, and the data were fit to the simple hyperbolic function given in eq 2 to yield an apparent reciprocal molar lipid affinity, K, as described previously (*31*).

$$f = \frac{aK[L]}{1 + K[L]} \quad (2)$$

where [L] is the concentration of accessible lipid, f is the fraction of C2 domain bound to the membrane, and a is a scaling factor.

Fluorescence measurements were taken at ambient temperature on a Jobin Yvon-Spex Fluorolog-3 model FL3 instrument (with both single, single and double, double excitation and emission monochromators), and the lamp-corrected emission spectra were collected. A Teflon-capped 300 μL minifluorimeter sample cell was used (McCarthy Scientific, Fullerton, CA) with continuous stirring, and 15 min incubations allowed between titration points. A narrow emission band-pass filter was selected, and the excitation wavelength was tuned to tryptophan to minimize photobleaching. Concentrations of C2B were determined using a Bradford assay.

EPR Spectroscopy. EPR spectra were recorded at room temperature using a Varian E-line Centuries series spectrometer fitted with a microwave preamplifier and an X-band loop-gap resonator (Medical Advances, Milwaukee, WI). Protein sample concentrations for EPR spectroscopy typically ranged from 20 to 300 μM, and the stock solution LUVs were diluted and used at a lipid concentration of 40−60 mM to ensure complete membrane binding and low surface densities of the protein. From the peak-to-peak line width of the EPR central resonance, δ, the scaled mobility, M_s, for the nitroxide was determined from the relation $M_s = (\delta^{-1} - \delta_i^{-1})/(\delta_m^{-1} - \delta_i^{-1})$ (*32*). Here δ_m and δ_i represent the line widths of the most mobile and least mobile R1 side chains, respectively, generally observed in proteins, and values of 2.1 and 8.4 G were taken for δ_m and δ_i, respectively.

Continuous-wave power saturation measurements were performed as described elsewhere (*15*). From these experiments, a collision parameter for O_2 (Π^{oxy}) and a collision parameter for NiEDDA (Π^{NiEDDA}) were determined (*33*). A depth parameter, Φ, was then calculated using the following expression:

$$\Phi = \ln\left(\frac{\Pi^{oxy}}{\Pi^{NiEDDA}}\right) \quad (3)$$

To provide quantitative estimates of nitroxide side chain motion, EPR spectra were simulated using the microscopic-order, macroscopic-disorder (MOMD) model developed by Freed and co-workers implemented in NLSL (*34*). As described elsewhere, the nitroxide R1 motion is constrained on protein surfaces and can be described by the X_4/X_5 model for R1 side chain motion (*35*). For these simulations, the principle values of the hyperfine tensor **A** were set to 6 G (A_{xx} and A_{yy}) and 37 G (A_{zz}), and 2.0076 (g_{xx}), 2.0050 (g_{yy}), and 2.0023 (g_{zz}) were used for the **g** tensor. The molecular frame of the nitroxide was displaced from the diffusion frame by tilt angles of 36.2° (β_D) and 4.0° (α_D). In the MOMD model, an isotropic correlation time, τ_c, was used with an order parameter, S, which defines a simple axially symmetric restoring potential used in the simulation [$S = -1/2(3\cos^2\theta - 1)$, where θ is the average angle between the protein fixed director and the z-axis of the diffusion tensor].

Modeling the Orientation and Position of the sytIC2B Domain. A model for the orientation and position of the synaptotagmin I C2B domain was generated from the EPR depth parameters using an approach described previously (*15*, *16*). Briefly, the averaged high-resolution NMR structure (PDB entry 1K5W) (*13*) with spin-labels attached was rotated through three Euler angles and translocated along the normal to a plane representing the level of the lipid phosphates until a best fit was obtained with the experimentally determined depth parameters (Φ values), depth calibration points, and an empirical form for the depth parameter Φ (eq 4). For the modeling, the spin-labels were appended to the high-resolution structure of C2B and placed into likely configurations based upon crystallographic studies of the R1 side chain (*36*). In this configuration, the first, second, and third dihedral angles are in a $g+$, $g+$, $g-$ conformation, except for residue 370, which was placed in a $g+$, t, $g-$ configuration due to steric constraints. A set of coordinates for the nitrogen atoms on the R1 side chain was then generated, and used for the modeling.[2]

It was previously shown that the dependence of Φ upon depth has the following empirical behavior:

$$\Phi = A\tanh[B(x - C)] + D \quad (4)$$

where x represents the distance of the label from the lipid

[2] The modeling procedure that is used to orient the C2 domain on the membrane interface places the label in a likely but static configuration and treats the protein as a rigid body. However, neither the nitroxides nor the C2 domain is static. The EPR spectra of R1 result from nanosecond time scale motion of the protein backbone and torsional oscillations about the fourth and fifth bonds linking the nitroxide to the peptide backbone (*35*). As a result, the distance estimates used for this modeling represent average depths of the nitroxide in the bilayer. The error estimates of the sytIC2B depth and orientation produced by this model include the uncertainty in the average nitroxide position in the static structure.

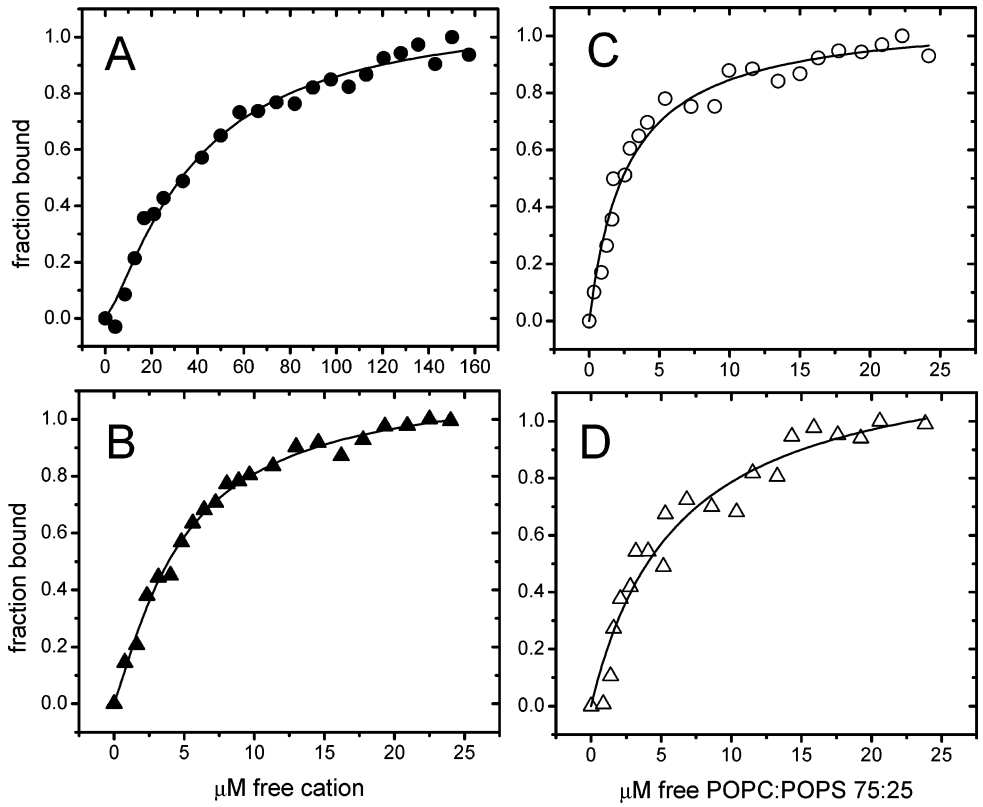

FIGURE 2: Tb^{3+} ion binding determined by the quenching of tryptophan fluorescence. Plot of fraction of bound vs free metal ion binding sites where the data are corrected for two cations bound at saturation. (A) Binding of Tb^{3+} to C2B in aqueous solution (●) where the fit (solid line) using eq 1 yields a K_d of 38 μM. (B) Binding of Tb^{3+} to C2B in the presence of 50 μM POPC/POPS (75:25) LUVs (▲) where the fit (solid line) yields a K_d of 5 μM. Concentrations of sytIC2B used were approximately 300 nM. The fits using the Hill approximation (eq 1) yielded a Hill coefficient of >1, consistent with cooperative binding of cation by protein. (C) Membrane binding of C2A as a function of lipid concentration (○) [POPC/POPS (75:25) LUVs]. The fit (solid line) to eq 2 yields a lipid binding affinity K of 3.7×10^5 M^{-1}. (D) Membrane binding of C2B as a function of lipid concentration (△) [POPC/POPS (75:25) LUVs]. The fit to eq 2 yields a K of 1.7×10^5 M^{-1}.

phosphates (positive values of x are inside the bilayer) and $A-D$ are constants (*15*, *16*). The values of A and D set the bulk values of Φ in water and hydrocarbon; C determines the position of the reflection point of the curve, and B determines the slope of the curve. The position and orientation of the domain were varied along with the quantities $D - A$, B, and C of eq 4 to find the best fit between the sytIC2B domain data and calibration points to the form of eq 4. The depth calibration points included data obtained previously for doxyl-labeled phosphatidylcholines (PC), bacteriorhodopsin (bR), and the sytIC2A domain (*15*, *16*). These calibration points provided values of Φ at known bilayer depths. Seven parameters were simultaneously varied to generate a self-consistent model describing both the depth dependence of Φ and the location of the C2B domain in the membrane. The model that is generated is constrained by the form of eq 4, Φ data for sytIC2B, the calibration points, the allowed configurations for the R1 side chain, and geometrical constraints imposed by the solution structure of the sytIC2B domain.

RESULTS

The SytIC2B Domain Binds with Micromolar Lipid Affinity to PC/PS Bilayers. Bacterially expressed, affinity-purified sytIC2B may contain a nucleic acid impurity, and in the presence of this impurity, Ca^{2+}-dependent membrane binding of the isolated C2B domain is not observed (*20*). For our studies with C2B, an ion exchange chromatography step was used to remove the bacterial nucleic acid contaminant, and the membrane binding of our purified C2B was tested using a Tb^{3+}-based assay (*16*, *31*). Shown in panels A and B of Figure 2 are titrations of the fraction of Tb^{3+} sites bound as a function of the free metal ion concentration. The data in panels A and B of Figure 2 were obtained from the decrease in protein fluorescence upon binding of Tb^{3+} to wild-type C2B in the presence and absence of membranes, respectively. The data were fit to eq 1 (solid lines) and indicate that Tb^{3+} has a K_d of 38 μM for C2B in the absence of membranes and a K_d of 5 μM in the presence of POPC/POPS (75:25) membranes. As discussed elsewhere, the metal affinities of the binding sites on C2 domains are enhanced upon membrane association, and the 7-fold enhancement in Tb^{3+} affinity observed here in the presence of membranes is a consequence of the membrane association of the domain (*31*).

The lipid affinities of the synaptotagmin I C2B and C2A domains for POPC/POPS (75:25) membranes were compared by titrating the C2 domain fluorescence with lipid vesicles at subsaturating concentrations of metal ion. Shown in panels C and D of Figure 2 are plots of the fraction of protein bound to membrane vesicles and fits of the data to eq 2. These data indicate that the C2B domain has an apparent molar binding affinity (K) of 1.7×10^5 M^{-1}, while C2A has an affinity of 3.7×10^5 M^{-1}. The data shown in Figure 2 indicate that the C2B preparations used here exhibit a metal ion and membrane affinity comparable to those of the C2A

Table 1: Tb^{3+} Binding Affinity of Wild-Type and Mutant sytIC2B in the Presence of POPC/POPS Membrane Vesicles[a]

C2B domain	K_d (μM)[b]	C2B domain	K_d (μM)[b]
wild-type	5 ± 0.1	G368R1	12 ± 1
V304R1	7.6 ± 0.3	K369R1	6.9 ± 0.4
G305R1	7.4 ± 0.8	N370R1	6.9 ± 0.2
T334R1	6.2 ± 0.2	A415R1	8.6 ± 0.4
I367R1	5.1 ± 0.1		

[a] Binding was assessed (see Figure 2) in the presence of POPC/POPS (75:25) LUVs at a lipid concentration of 50 μM. [b] K_d is the apparent dissociation constant for binding of Tb^{3+} to sytIC2 (see eq 1), and the value of n was set to 1.26.

domain. To determine whether additional metal ion or small nonprotein contaminants might be influencing the results, our C2B domain preparation was exhaustively dialyzed and the titrations in Figure 2A and 2B repeated. Tb^{3+} binding affinities identical to those obtained before dialysis were found in the absence and presence of membranes.

Ca^{2+}-Binding Loops of C2B Interact with the Membrane Interface. A series of single-cysteine mutants of the C2B domain were produced, purified, and chemically modified to attach the R1 side chain. These spin-labels are located on the exposed surface of the domain in or near the membrane binding loops. Each of the spin-labeled C2B domain mutants was tested to determine whether each was properly folded and bound membranes in a metal ion-dependent fashion using the fluorescence Tb^{3+} assay shown in Figure 2B. Table 1 is a list of the K_d values (see eq 1) that were obtained for wild-type C2B and each mutant in the presence of POPC/POPS (75:25) LUVs. The data indicate that each R1 mutant is folded and binds POPC/POPS membranes. The metal ion affinities of these C2B mutants in the presence of membranes vary by a factor of less than 3, and this is comparable to the range of affinities measured for a series of spin-labeled mutants in the sytIC2A domain (*16*). The fact that each of these mutants is functional is consistent with the observation that R1 side chains, when placed on externally facing protein sites, are not highly perturbing (*37*).

Shown in Figure 3 are EPR spectra from the eight R1-labeled C2B mutants in the presence of Ca^{2+}, with and without membranes composed of POPC and POPS (75:25). These spectra have been normalized so that their amplitudes provide an approximate measure of the dynamics of the spin-label side chain (more mobile spin-labels have larger normalized amplitudes). In the absence of membranes, the EPR spectra are consistent with the expected secondary structure. In flexible loops that connect elements of secondary structure, the EPR line shapes from the R1 side chain are expected to be substantially motionally averaged (*37*), and the spectra in Figure 3 indicate that this is the case. The EPR spectra from the R1 side chain at most loop sites, for example, positions 304, 305, 367, and 369, have small line widths and large amplitudes in the absence of membranes, indicating that the R1 side chain is attached to a highly dynamic protein segment. Most of these spectra may be accurately simulated by a label having a 1 ns isotropic correlation time and an order parameter, S_{20}, near zero, consistent with motion expected for a label attached to a highly flexible protein backbone (*38*). At a few loop sites, for example, positions 368 and 370, the EPR spectra are broader and lower in amplitude than at the other loop sites.

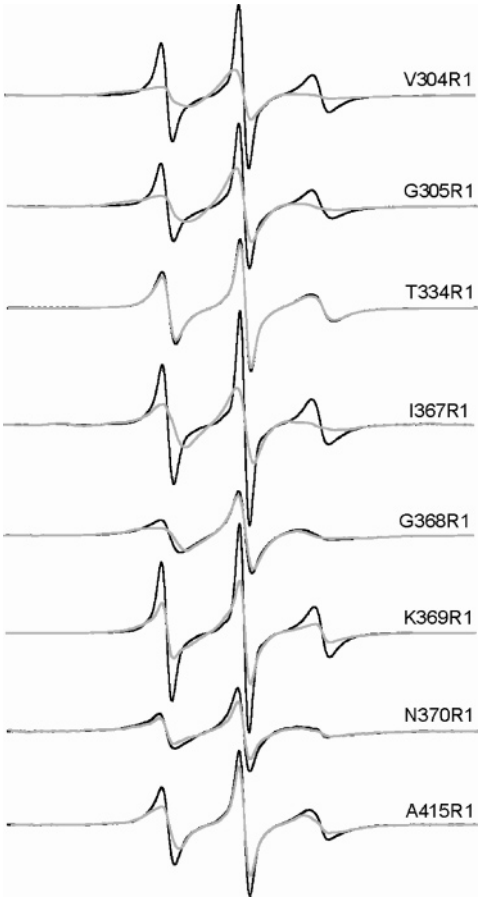

FIGURE 3: X-Band EPR spectra of spin-labeled sytIC2B domain mutants recorded in aqueous solution in the presence of Ca^{2+} (black lines) and bound to POPC/POPS (75:25) vesicles (gray lines). The loss in intensity and broadening of the EPR spectra reflect a loss of motional averaging upon membrane binding of the domain (see the text). Spectra are 100 G scans.

These line shapes can be simulated with somewhat longer correlation times (1.5−2 ns) and a non-zero order parameter ($S_{20} \sim 0.3$). This slower rate and improved ordering are expected, because the label at these sites appears to be more sterically constrained than at other loop sites in the high-resolution structure of C2B. The spectrum from the R1 side chain at position 415 within the C-terminal helix of C2B does not have an EPR spectrum typical of a labeled helix site (*35*, *39*). It is more motionally averaged than expected for R1 on a helix, and indicates that this C-terminal helix is not well-ordered.

In the presence of Ca^{2+} and membranes composed of POPC and POPS (75:25) (gray lines), the line widths increase and the amplitudes decrease for many of these EPR spectra, indicating reduced motional averaging of the magnetic interactions of R1. The most dramatic line shape changes are observed for the spectra from V304R1 and G305R1 in loop 1, and I367R1 and K369R1 in loop 3, while the EPR spectrum of T334R1 in loop 2 shows little change when POPC/POPS bilayers are present. These line shape changes are all reversed upon the removal of Ca^{2+} by addition of EDTA (data not shown). Although these changes in EPR line shape alone do not necessarily indicate membrane insertion of the label, similar line shape changes observed for other C2 domains upon membrane binding have been shown to result from membrane insertion of the R1 side chain

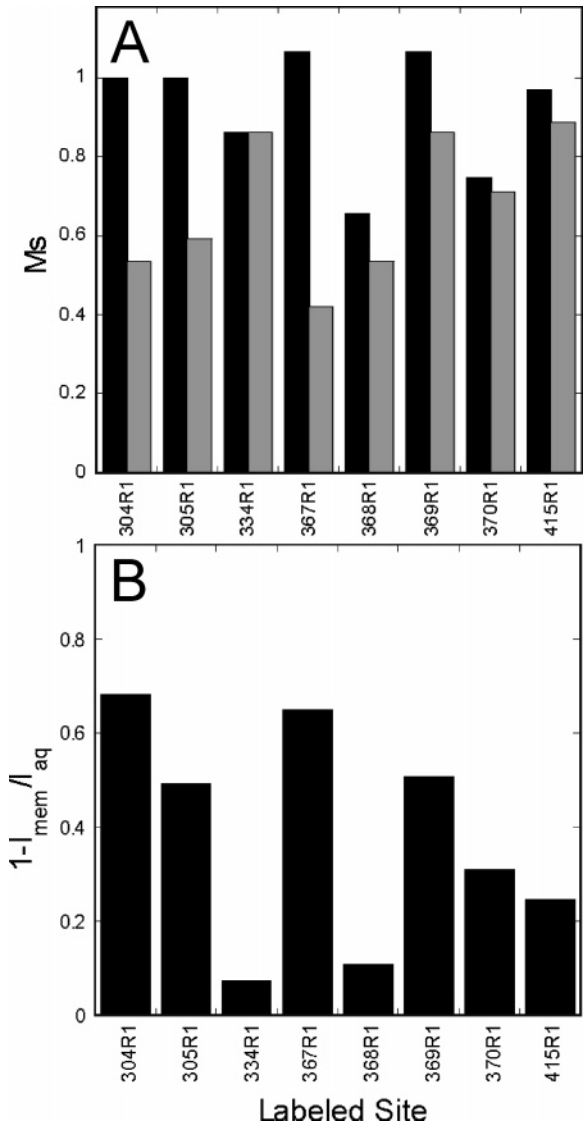

FIGURE 4: (A) Scaled mobilities, M_s, determined from the spectra shown in Figure 3 using δ_m and δ_i values of 2.1 and 8.4 G, respectively. The M_s values indicate that the labeled loop sites of the sytIC2B domain are among the most mobile sites found in proteins. (B) Fractional changes in normalized amplitudes upon membrane binding. The normalized intensity provides a qualitative measure of the motional averaging of the nitroxide. A value for $1 - I_{mem}/I_{aq}$ of 0 corresponds to no loss in EPR spectra intensity upon membrane binding. A value of 1 corresponds to the complete loss in normalized intensity upon binding.

(*15*, *16*). Thus, it is likely that the changes observed in Figure 3 result from the binding of the C2B domain and insertion of the spin-labeled side chain into the bilayer. It should be noted that the aqueous EPR line shapes of spin-labeled C2B mutants are not altered by agents that increase solution viscosity, such as Ficoll 400, indicating that a reduction in the overall tumbling rate of C2B upon membrane binding is not responsible for the observed line broadening.

Shown in Figure 4A are the scaled mobilities, M_s, obtained from EPR spectra in Figure 3 in the presence and absence of POPC/POPS vesicles. The values of M_s provide a qualitative measure of the motion of the nitroxide side chain (*32*), where M_s values of 0 and 1 correspond to the least and most mobile EPR line shapes obtained from the R1 side chain in proteins, respectively. In the absence of membranes (black bars), the scaled mobilities for most sites have values close to 1, indicating that these labeled sites have some of the most mobile EPR line shapes seen in proteins. In the presence of PC/PS bilayers (gray bars), the values of M_s decrease at most sites, with the largest decreases for spin-labels within loops 1 and 3. The normalized intensity of the central EPR resonance also provides a qualitative measure of the motion of the R1 side chain, and in Figure 4B, the loss in intensity upon membrane binding is plotted for each C2B spin-label. These data also indicate that the greatest decrease in motion takes place for labels in Ca^{2+}-binding loops 1 and 3 when C2B binds POPC/POPS bilayers. The changes seen in the scaled mobilities for the labeled loop sites upon membrane binding have a pattern similar to those found previously for the C2A domain of syntaptotagmin I (*16*); however, the values of M_s for the nitroxide labels on C2B appear to be higher than the value of those attached to C2A. This may indicate that the Ca^{2+}-binding loops in C2B have greater amplitudes or rates of motion compared to those in C2A.

Table 2: Collision and Depth Parameters for sytIC2B[a]

mutant	Π^{oxy}	Π^{NiEDDA}	Φ	mutant	Π^{oxy}	Π^{NiEDDA}	Φ
V304R1	0.23	0.97	−1.5	G368R1	0.21	1.3	−1.8
G305R1	0.21	0.47	−0.7	K369R1	0.17	1.7	−2.3
T334R1	0.30	2.69	−2.2	N370R1	0.18	1.6	−2.2
I367R1	0.31	0.40	−0.2	A415R1	0.26	2.4	−2.2

[a] Collision data for the C2B domain bound to PC/PS (75:25) LUVs. The uncertainty in the Π^{oxy} value is on the order of ±0.05. The uncertainty in Π^{NiEDDA} is on the order of ±0.4. Values of Φ are determined from eq 3. The values of Φ for sites 334, 369, 370, and 415 are less than −2.0 and are close to the bulk aqueous value for Φ. At positions greater than 5 Å from the membrane surface, Φ assumes its bulk value and becomes insensitive to distance.

The Ca^{2+}-Binding Loops of C2B Penetrate the Membrane Interface. Power saturation experiments were performed on each of the spin-labeled mutants to obtain a depth parameter Φ as described above (see Experimental Procedures). Shown in Table 2 are the collision parameters and the depth parameters (eq 3) obtained for each of the R1-labeled C2B domain mutants. These results show that four of the labeled sites are near or within the lipid bilayer interface, and that four of the labeled sites have values that are near the values obtained for sites in bulk aqueous phases.

As described above (see Experimental Procedures), these depth data were used together with calibration data from doxyl-labeled PCs, spin-label bacteriorhodopsin (bR), and other protein calibration points to generate a model for the C2B domain at the membrane interface. Shown in Figure 5 is a plot of the fit and the distance dependence of the depth parameter obtained by modeling the orientation of the domain using the power saturation data shown in Table 2. The best fit parameters obtained for the depth dependence of Φ (eq 4) were 3.2, 0.11, 7.1, and 0.9 for $A-D$, respectively. These values, which define the form of $\Phi(x)$, are very close to the values obtained from a similar fit using the data and a molecular model for C2A (*16*).

Figure 6 shows two views of the model obtained for the C2B domain which differ by a 90° rotation about the membrane normal. Our EPR membrane-bound model indicates that the backbone of Ca^{2+}-binding loops 1 and 3 of the domain is inserted into the bilayer interface, with the backbone of Ca^{2+}-binding loop 2 and the two Ca^{2+} ion sites lying close to a plane defined by the level of the lipid phosphates.

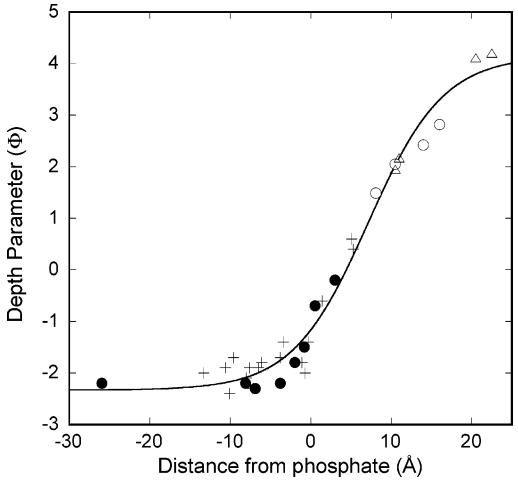

FIGURE 5: Depth calibration curve showing the fit of eq 4 and the dependence of Φ on position from the lipid phosphates. The *y*-axis values (Φ) for the sytIC2B data (●) are experimentally determined values (Table 2), and the *x*-axis values (distances) are generated from the high-resolution solution structure of sytIC2B in its best fit position and orientation. Calibration points generated previously from bacteriorhodopsin (△), doxyl spin-labeled lipids (○), and the sytIC2A domain (+) (*16*) were used in the fit (see Experimental Procedures).

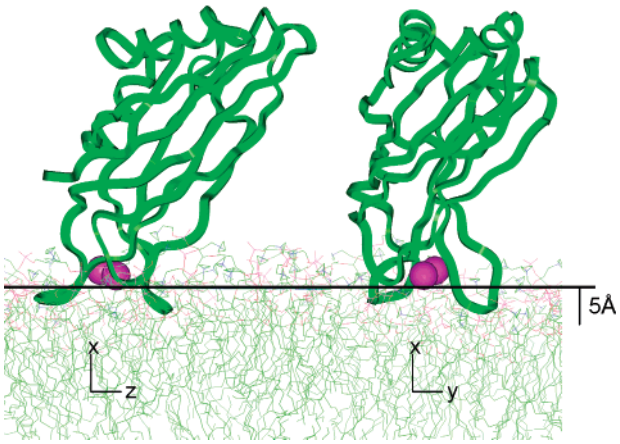

FIGURE 6: Orientation and position of the synaptotagmin I C2B on POPC/POPS bilayers [the high-resolution NMR structure (PDB entry 1KW5) was used to produce this model]. The horizontal line represents the plane defined by the lipid phosphates. The best fit position corresponds to successive Euler angle rotations for ϕ (*z*-axis), θ (*x*′-axis), and ψ (*z*′-axis) of 188°, 219°, and 22°, respectively, and a displacement of structure along the *x*-axis of −19.8 Å. These rotations and displacement are carried out using the center of mass of the protein on the local coordinate frame defined by the PDB entry, where the bilayer phosphates lie in the *y*−*z* plane. Two views differing by a 90° rotation about the bilayer normal are shown. The protein is shown docked to a bilayer (note the bilayer simulation was performed in the absence of protein) (*42*).

A number of sources of error are inherent in this modeling strategy. This approach treats the average NMR-derived structure as a rigid body and assumes that there are no changes in structure upon membrane binding. The approach also assumes that eq 4 represents the correct form for the depth dependence for the parameter Φ. Both of these assumptions appear to be reasonable. Equation 4 works well for two other membrane-penetrating domains (*15*, *16*), suggesting that this dependence is appropriate. If large structural changes in C2B were taking place upon membrane

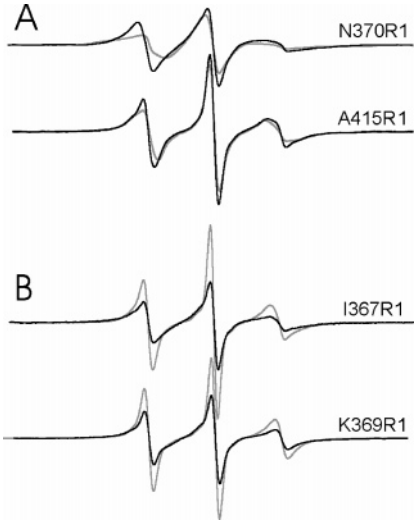

FIGURE 7: (A) Comparison of the EPR spectra for R1 at positions 370 and 415 obtained for sytIC2B fully bound to membranes under two different sets of conditions: with Ca^{2+} bound to POPC/POPS (75:25) LUVs (black lines) and with Ca^{2+} bound to POPC/POPS/PI(4,5)P_2 (75:24:1) LUVs (gray lines). (B) Comparison of the EPR spectra obtained for R1 at positions 367 and 369 without Ca^{2+} in aqueous solution (gray lines) and without Ca^{2+} in the presence of POPC/POPS/PI(4,5)P2 (75:24:1) LUVs (black lines).

binding, the fit obtained for most of the labeled sites to the expected behavior of Φ(*x*) (see Figure 5) should not be seen. The conformation of the R1 side chain on the protein surface is another source of error in this modeling approach. From the crystal structures of the R1 label attached to T4 lysozyme (*36*), it has been shown that the first two dihedral angles from the backbone are well-defined, while the third dihedral angle may be found with orientations of either +90° or −90°. When rotations about X_3 were explored, it was found that +90° produces the best fit to the data (consistent with the finding that this is the rotomeric state with the lowest energy). Rotation about X_4 can add an additional distance variation of approximately 3 Å at any one site. As a result of these uncertainties, we estimate that the Euler angles defining the orientation of the domain are accurate to within ±10° and that the depth of penetration of the domain at the interface has an uncertainty of ±3 Å.

The EPR Spectra from Membrane-Bound SytIC2B Are Altered by the Presence of PI(4,5)P_2. As indicated above, the isolated C2B domain of synaptotagmin has been reported to bind membranes containing PI(4,5)P_2 and to assume a different orientation on PC/PS bilayers when PI(4,5)P_2 is present (*23*). Shown in Figure 7A are EPR spectra for two spin-labeled C2B mutants when fully bound to membranes formed from either POPC and POPS (25:75) (gray lines) or POPC, POPS, and PI(4,5)P_2 (74:25:1) (black lines) in the presence of Ca^{2+}. The presence of PI(4,5)P_2 alters the EPR spectra from these labeled sites, and the line shapes at both sites indicate that there is an enhanced motional averaging of R1. One likely interpretation for the differences seen in Figure 7A is that the interaction of C2B with the PC/PS interface is altered by the presence of PI(4,5)P_2. Work is currently underway to measure depth parameters and produce a model for C2B bound to the interface of membranes containing PI(4,5)P_2.

EPR Spectroscopy Indicates that C2B Binds Membranes Containing PI(4,5)P_2 in the Absence of Ca^{2+}. The sytIC2B

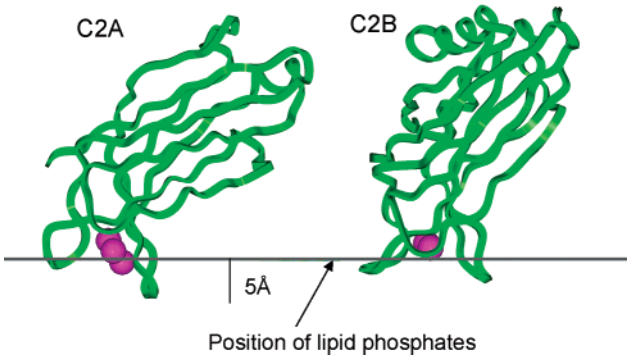

FIGURE 8: Comparison of the membrane positions of sytIC2A and sytIC2B. The sytIC2A position was published previously (*16*). Both domains interact through loops 1 and 3, and the Ca^{2+} ion binding sites for each domain reside at a similar depth in the bilayer interface. The C2B domain has an orientation slightly different from that of C2A. The β-strands of the C2B domain make a smaller angle with respect to the bilayer normal than those of C2A.

domain has been reported to bind to membranes containing $PI(4,5)P_2$ in the absence of Ca^{2+}(*23*), and EPR spectra obtained from spin-labeled sites on C2B are consistent with this finding. Figure 7B compares the EPR spectra of two spin-labeled C2B mutants without Ca^{2+} under two conditions: in aqueous solution (gray line) and in the presence of POPC/POPS/$PI(4,5)P_2$ (74:25:1) membrane vesicles (black line). At these two sites (which are both in loop 3), the EPR line shapes indicate that there is a decrease in motional averaging of the R1 side chain in the presence of $PI(4,5)P_2$ containing membranes in the absence of Ca^{2+}. No significant changes in the EPR line shape are seen for labels in loop 1 or 2, and no change in line shape takes place without Ca^{2+} when POPC/POPS (75:25) membranes are added (data not shown). As indicated above, the changes in the EPR spectra at these exposed loop sites are most likely due to membrane association, and the simplest interpretation of the spectra shown in Figure 7B is that sites in loop 3 of C2B interact with POPC/POPS/$PI(4,5)P_2$ membranes in the absence of Ca^{2+}.

DISCUSSION

In the work described here, SDSL was used to determine the position and orientation of the sytIC2B domain on membranes composed of POPC and POPS (75:25). The model shown in Figure 6 indicates that Ca^{2+}-binding loops 1 and 3 penetrate the membrane interface with both Ca^{2+} ions localized near the plane of the lipid phosphates. A comparison of the model produced here for the isolated C2B domain [sytI(249−421)] with that found previously for the isolated C2A domain [sytI(96−265)] is shown in Figure 8. On membrane surfaces composed of POPC and POPS (75:25), the two domains have similar interactions with the interface. Both domains interact with the bilayer through their first and third Ca^{2+}-binding loops, and both domains penetrate the bilayer to approximately the same extent, as judged by the position of the Ca^{2+}-binding loops and the coordinated Ca^{2+} ions. The β-strands of sytIC2B have a slightly different orientation with respect to the bilayer normal than those of C2A. For example, β-strand 4 in sytIC2B is tilted approximately 30° closer to vertical compared to strand 4 of sytIC2A.

The Tb^{3+} fluorescence measurements taken here (Figure 2) indicate that the C2B domain has a metal ion and membrane affinity for POPC/POPS membranes comparable to those observed for the C2A domain. C2B is observed to have a K_d for Tb^{3+} binding of 5 ± 0.1 μM in the presence of POPC and POPS (75:25); previously, the K_d for C2A was found to be 8 ± 2 μM in the presence of POPC and POPS (75:25) (*16*). As shown in Figure 2, the lipid binding affinities (K) of C2A and C2B for POPC/POPS (75:25) membranes were also found to be very similar, and this result is consistent with previous measurements using either fluorescence energy transfer or vesicle binding to the immobilized C2 domain (*13*).

The results obtained here demonstrate that the isolated C2B domain penetrates PC/PS bilayers, and this result contrasts with work indicating that the isolated C2B domain does not penetrate significantly into POPC/POPS bilayers unless C2B is expressed in tandem with the C2A domain (*23*, *24*). In this earlier work, the fluorescent probe AEDANS was placed at either position 304 or 367 (Ca^{2+}-binding loop 1 or 3, respectively) on the isolated C2B domain. The emission spectrum from these probes failed to show changes in quantum yield or emission wavelength in the presence of Ca^{2+} and POPC/POPS membranes, and it was concluded that these sites do not penetrate into the bilayer. In contrast, EPR spectra for both V304R1 and I367R1 show changes in line shape characteristic of membrane association and have depth parameters indicating localization at or within the bilayer interface (Figure 3 and Table 2). Preliminary EPR data we have obtained for C2B when expressed in tandem with C2A are qualitatively consistent with this previous fluorescence work and indicate that C2B penetrates more deeply into PC/PS bilayers when it is attached to C2A (D. E. Zbell and D. S. Cafiso, unpublished results).

Phosphatidylinositol 4,5-bisphosphate is a lipid that plays a critical role in fusion (*40*, *41*); however, the exact molecular role of $PI(4,5)P_2$ is not understood. $PI(4,5)P_2$ may have multiple roles in fusion as it interacts with many membrane binding domains and protein components involved in fusion. Conceivably, $PI(4,5)P_2$ may function to alter the membrane interactions made by synaptotagmin. For example, $PI(4,5)P_2$ might target the attachment of synaptotagmin C2B to the plasma membrane surface, or it might trigger conformational changes in the C2 domains of synaptotagmin that mediate its interactions with SNAREs.

The results obtained here indicate that the C2A and C2B domains of sytI have similar Ca^{2+}-dependent interactions with phospholipid bilayers containing PC and PS; however, C2B appears to have alternate modes of binding to PC/PS membranes containing $PI(4,5)P_2$. When some of the labeled sites are bound to PC and PS, with and without $PI(4,5)P_2$, changes in the EPR spectra are observed in the presence of $PI(4,5)P_2$. These data (Figure 7A) indicate that $PI(4,5)P_2$ alters the Ca^{2+}-dependent interactions of C2B with PC/PS surfaces. The EPR spectra shown in Figure 7B suggest that C2B binds to POPC/POPS/$PI(4,5)P_2$ membranes in the absence of Ca^{2+}. Evidence for contact with the membrane interface is obtained from spin-labeled sites in loop 3, and the interaction of this loop with the interface is consistent with an orientation for C2B that would place the polybasic region of the domain close to the membrane interface. This is consistent with a recent report that the C2B domain binds to PC/PS/$PI(4,5)P_2$ membranes in a Ca^{2+}-independent fashion (*23*). We are at present making additional measurements to

confirm this interpretation and to determine the membrane-bound position of sytIC2B in membranes containing PI(4,5)-P_2.

In summary, the affinity, orientation, and depth of membrane penetration of the isolated C2B domain of synaptotagmin on membrane interfaces formed from POPC and POPS have been determined. The C2B domain is found to have a similar metal ion affinity in the presence of POPC/POPS membranes as does the C2A domain. The C2B domain penetrates the interface of POPC/POPS (75:25) membranes so that the polypeptide backbones of Ca^{2+}-binding loops 1 and 3 are inserted into the bilayer. Ca^{2+}-binding loop 2 is also positioned near the interface, and the Ca^{2+} binding sites on the domain reside near a plane defined by the level of the lipid phosphates. This orientation and position are similar to that found for the sytIC2A domain, and indicate that C2A and C2B interact similarly with POPC/POPS bilayers.

ACKNOWLEDGMENT

We thank Dr. Ken G. Victor for his assistance with modeling the orientation of the C2B domain and Dr. Gail E. Fanucci for helpful discussions regarding the manuscript.

REFERENCES

1. Koh, T. W., and Bellen, H. J. (2003) Synaptotagmin I, a Ca^{2+} sensor for neurotransmitter release, *Trends Neurosci. 26*, 413−422.
2. Tucker, W. C., and Chapman, E. R. (2002) Role of synaptotagmin in Ca^{2+}-triggered exocytosis, *Biochem. J. 366*, 1−13.
3. Fernandez-Chacon, R., Konigstorfer, A., Gerber, S. H., Garcia, J., Matos, M. F., Stevens, C. F., Brose, N., Rizo, J., Rosenmund, C., and Sudhof, T. C. (2001) Synaptotagmin I functions as a calcium regulator of release probability, *Nature 410*, 41−49.
4. Fernandez-Chacon, R., Shin, O. H., Konigstorfer, A., Matos, M. F., Meyer, A. C., Garcia, J., Gerber, S. H., Rizo, J., Sudhof, T. C., and Rosenmund, C. (2002) Structure/function analysis of Ca^{2+} binding to the C2A domain of synaptotagmin 1, *J. Neurosci. 22*, 8438−8446.
5. Robinson, I. M., Ranjan, R., and Schwarz, T. L. (2002) Synaptotagmins I and IV promote transmitter release independently of Ca^{2+} binding in the C(2)A domain, *Nature 418*, 336−340.
6. Mackler, J. M., Drummond, J. A., Loewen, C. A., Robinson, I. M., and Reist, N. E. (2002) The C2B Ca^{2+}-binding motif of synaptotagmin is required for synaptic transmission *in vivo*, *Nature 418*, 340−344.
7. Wang, C. T., Lu, J. C., Bai, J., Chang, P. Y., Martin, T. F., Chapman, E. R., and Jackson, M. B. (2003) Different domains of synaptotagmin control the choice between kiss-and-run and full fusion, *Nature 424*, 943−947.
8. Tucker, W. C., Weber, T., and Chapman, E. R. (2004) Reconstitution of Ca^{2+}-regulated membrane fusion by synaptotagmin and SNAREs, *Science 304*, 435−438.
9. Nalefski, E. A., and Falke, J. J. (1996) The C2 domain calcium-binding motif: Structural and functional diversity, *Protein Sci. 5*, 2375−2390.
10. Nalefski, E. A., Wisner, M. A., Chen, J. Z., Sprang, S. R., Fukuda, M., Mikoshiba, K., and Falke, J. J. (2001) C2 domains from different Ca^{2+} signaling pathways display functional and mechanistic diversity, *Biochemistry 40*, 3089−3100.
11. Rizo, J., and Sudhof, T. C. (1998) C2-domains, structure and function of a unversal Ca^{2+}-binding domain, *J. Biol. Chem. 273*, 15879−15882.
12. Hurley, J. H., and Misra, S. (2000) Signaling and subcelluar targeting by membrane-binding domains, *Annu. Rev. Biophys. Biomol. Struct. 29*, 49−79.
13. Fernandez, I., Arac, D., Ubach, J., Gerber, S. H., Shin, O., Gao, Y., Anderson, R. G., Sudhof, T. C., and Rizo, J. (2001) Three-dimensional structure of the synaptotagmin 1 C2B-domain: Synaptotagmin 1 as a phospholipid binding machine, *Neuron 32*, 1057−1069.
14. Ball, A., Nielsen, R., Gelb, M. H., and Robinson, B. H. (1999) Interfacial membrane docking of cytosolic phospholipase A2 C2 domain using electrostatic potential-modulated spin relaxation magnetic resonance, *Proc. Natl. Acad. Sci. U.S.A. 96*, 6637−6642.
15. Frazier, A. A., Wisner, M. A., Malmberg, N. J., Victor, K. G., Fanucci, G. E., Nalefski, E. A., Falke, J. J., and Cafiso, D. S. (2002) Membrane orientation and position of the C2 domain from cPLA2 by site-directed spin labeling, *Biochemistry 41*, 6282−6292.
16. Frazier, A. A., Roller, C. R., Havelka, J. J., Hinderliter, A., and Cafiso, D. S. (2003) Membrane-bound orientation and position of the synaptotagmin I C2A domain by site-directed spin labeling, *Biochemistry 42*, 96−105.
17. Malmberg, N. J., Van Buskirk, D. R., and Falke, J. J. (2003) Membrane-docking loops of the cPLA2 C2 domain: Detailed structural analysis of the protein-membrane interface via site-directed spin-labeling, *Biochemistry 42*, 13227−13240.
18. Kohout, S. C., Corbalan-Garcia, S., Gomez-Fernandez, J. C., and Falke, J. J. (2003) C2 domain of protein kinase Cα: Elucidation of the membrane docking surface by site-directed fluorescence and spin labeling, *Biochemistry 42*, 1254−1265.
19. Desai, R. C., Vyas, B., Earles, C. A., Littleton, J. T., Kowalchyck, J. A., Martin, T. F., and Chapman, E. R. (2000) The C2B domain of synaptotagmin is a Ca^{2+}-sensing module essential for exocytosis, *J. Cell Biol. 150*, 1125−1136.
20. Ubach, J., Lao, Y., Fernandez, I., Arac, D., Sudhof, T. C., and Rizo, J. (2001) The C2B domain of synaptotagmin I is a Ca^{2+}-binding module, *Biochemistry 40*, 5854−5860.
21. Creutz, C. E., Tomsig, J. L., Snyder, S. L., Gautier, M. C., Skouri, F., Beisson, J., and Cohen, J. (1998) The copines, a novel class of C2 domain-containing, calcium-dependent, phospholipid-binding proteins conserved from Paramecium to humans, *J. Biol. Chem. 273*, 1393−1402.
22. Schulz, T. A., and Creutz, C. E. (2004) The tricalbin C2 domains: Lipid-binding properties of a novel, synaptotagmin-like yeast protein family, *Biochemistry 43*, 3987−3995.
23. Bai, J., Tucker, W. C., and Chapman, E. R. (2004) PIP2 increases the speed of response of synaptotagmin and steers its membrane-penetration activity toward the plasma membrane, *Nat. Struct. Mol. Biol. 11*, 36−44.
24. Bai, J., Wang, P., and Chapman, E. R. (2002) C2A activates a cryptic Ca^{2+}-triggered membrane penetration activity within the C2B domain of synaptotagmin I, *Proc. Natl. Acad. Sci. U.S.A. 99*, 1665−1670.
25. Altenbach, C., Greenhalgh, D. A., Khorana, H. G., and Hubbell, W. L. (1994) A collision gradient-method to determine the immersion depth of nitroxides in lipid bilayers. Application to spin-labeled mutants of bacteriorhodopsin, *Proc. Natl. Acad. Sci. U.S.A. 91*, 1667−1671.
26. Guan, K. L., and Dixon, J. E. (1991) Eukaryotic proteins expressed in *Escherichia coli*: An improved thrombin cleavage and purification procedure of fusion proteins with glutathione S-transferase, *Anal. Biochem. 192*, 262−267.
27. Sambrook, J., Fritsch, E. F., and Maniatis, T. (1989) *Molecular Cloning: A Laboratory Manual*, Cold Spring Harbor Press, Plainview, NY.
28. Martin, R. B., and Richardson, F. S. (1979) Lanthanides as probes for calcium in biological systems, *Q. Rev. Biophys. 12*, 181−209.
29. Borin, G., Ruzza, P., Rossi, M., Calderan, A., Marchiori, F., and Perrion, E. (1989) Conformation and ion binding properties of peptides related to calcium binding domain III of bovine brain calmodulin, *Biopolymers 28*, 353−369.
30. Selvin, P. R. (2002) Principles and biophysical applications of lanthanide-based probes, *Annu. Rev. Biophys. Biomol. Struct. 31*, 275−302.
31. Hinderliter, A., Almeida, P. F. F., Creutz, C. E., and Biltonen, R. L. (2001) Domain formation in a fluid mixed lipid bilayer modulated through binding of the C2 protein motif, *Biochemistry 40*, 4181−4191.
32. Hubbell, W. L., Cafiso, D. S., and Altenbach, C. (2000) Conformational changes with site directed spin labeling, *Nat. Struct. Biol.* (in press).
33. Farahbakhsh, Z. T., Altenbach, C., and Hubbell, W. L. (1992) Spin-labeled cysteines as sensors for protein−lipid interaction and conformation in rhodopsin, *Photochem. Photobiol. 56*, 1019−1033.
34. Budil, D. E., Lee, S., Saxena, S., and Freed, J. H. (1996) Nonlinear-least-squares analysis of slow motion EPR spectra in one and two

dimensions using a modified Levenberg−Marquardt algorithm, *J. Magn. Reson., Ser. A 120*, 155−189.
35. Columbus, L., Kalai, T., Jeko, J., Hideg, K., and Hubbell, W. L. (2001) Molecular motion of spin labeled side chains in α-helices: Analysis by variation of side chain structure, *Biochemistry 40*, 3828−3846.
36. Langen, R., Oh, K. J., Cascio, D., and Hubbell, W. L. (2000) Crystal structures of spin-labeled T4 lysozyme mutants: Implications for the interpretation of EPR spectra in terms of structure, *Biochemistry 39*, 8396−8405.
37. Mchaourab, H., Lietzow, M., Hideg, K., and Hubbell, W. (1996) Motion of spin-labeled side-chains in T4 lysozyme. I. Correlation with protein structure and dyanmics, *Biochemistry 35*, 7692−7704.
38. Columbus, L., and Hubbell, W. L. (2004) Mapping backbone dynamics in solution with site-directed spin labeling: GCN4-58 bZip free and bound to DNA, *Biochemistry 43*, 7273−7287.
39. Columbus, L., and Hubbell, W. L. (2002) A new spin on protein dynamics, *Trends Biochem. Sci. 27*, 288−295.
40. Martin, T. F. (2001) PI(4,5)P2 regulation of surface membrane traffic, *Curr. Opin. Cell Biol. 13*, 493−499.
41. Martin, T. F. J. (1997) Stages of regulated exocytosis, *Trends Cell Biol. 7*, 271−276.
42. Tieleman, D. P., Berendsen, H. J., and Sansom, M. S. (1999) Surface binding of alamethicin stabilizes its helical structure: Molecular dynamics simulations, *Biophys. J. 76*, 3186−3191.

BI048370D